

JGR Biogeosciences

RESEARCH ARTICLE

10.1029/2018JG004959

Key Points:

- Phytoplankton much prefer ammonium over nitrate and nitrite in eutrophic estuary
- Oxidation of ammonia was significantly higher than nitrite in turbid water
- $\delta^{15}\text{N}\text{-NO}_2^-$ nicely reveals multiple nitrogen end-members

Supporting Information:

- Supporting Information S1

Correspondence to:

S.-J. Kao,
 sjkao@xmu.edu.cn

Citation:

Yan, X., Wan, X. S., Liu, L., Xu, M. N., Tan, E., Zheng, Z., et al. (2019). Biogeochemical dynamics in a eutrophic tidal estuary revealed by isotopic compositions of multiple nitrogen species. *Journal of Geophysical Research: Biogeosciences*, 124, 1849–1864. <https://doi.org/10.1029/2018JG004959>







Received 27 NOV 2018

Accepted 22 MAY 2019

Accepted article online 7 JUN 2019

Published online 6 JUL 2019

Biogeochemical Dynamics in a Eutrophic Tidal Estuary Revealed by Isotopic Compositions of Multiple Nitrogen Species

Xiuli Yan^{1,2} , Xianhui Sean Wan² , Li Liu², Min Nina Xu³ , Ehui Tan² , Zhenzhen Zheng³, Wenbin Zou², Li Tian², Da-Wei Li⁴, Thomas W. Trull⁵ , and Shuh-Ji Kao² 

¹Institute of Marine Science and Guangdong Provincial Key Laboratory of Marine Biotechnology, College of Science, Shantou University, Shantou, China, ²State Key Laboratory of Marine Environmental Science, College of Ocean and Earth Sciences, Xiamen University, Xiamen, China, ³State Key Laboratory of Marine Environmental Science, College of the Environment and Ecology, Xiamen University, Xiamen, China, ⁴Key Laboratory of Marine Chemistry Theory and Technology, Ministry of Education, Ocean University of China, Qingdao, China, ⁵CSIRO Oceans and Atmosphere, Hobart, Tasmania, Australia

Abstract Estuaries sit at the land-ocean boundary and act as natural reactors for nitrogen (N) transformations among numerous forms. Superimposing onto physical mixing, biological processes lead to nonconservative N behavior in estuaries. Under the coinfluences of biological alteration and multiple end-members, however, some N species can exhibit apparent conservation. To explore N dynamics and potential mechanisms that modulate the mixing behaviors, we measured concentrations and natural isotopic compositions of multiple N species (nitrate: NO_3^- , nitrite: NO_2^- , ammonium: NH_4^+ , and particulate nitrogen) in a typical eutrophic estuary in southern China. Additionally, N uptake and oxidation rates were measured by using isotope labelling techniques to evaluate processes potentially offsetting the conservative mixing of specific N pools. We found that NO_3^- followed conservative two end-member mixing with dual isotopes varying in a narrow range ($<1\text{--}2\text{‰}$) due to low microbial preferences. Moreover, $\delta^{15}\text{N}\text{-NO}_2^-$ revealed a nonconservative pattern with an involvement of multiple end-members. The dominant N transformation processes shifted downstream. In the upper estuary, ammonia oxidation ($\sim 20 \mu\text{mol L}^{-1} \text{day}^{-1}$) dominated NH_4^+ removal and was accompanied by NO_2^- accumulation. In the middle-lower estuary, NH_4^+ uptake became dominant, with phytoplankton showing strong preference for it over NO_3^- and NO_2^- . Based on measured NH_4^+ uptake rates ($9.1\text{--}12.5 \mu\text{mol L}^{-1} \text{day}^{-1}$ in the light and $0.9 \mu\text{mol L}^{-1} \text{day}^{-1}$ in the dark), short water residence time (<1 day) was required to maintain the conservative mixing. Coupling N isotopes in multiple nitrogen species with measurements of N uptake and nitrification, we successfully uncovered N dynamics and distinguished biological processes from physical mixing.

1. Introduction

Nitrogen (N) is a pivotal element to regulate marine primary productivity (Moore et al., 2013). Globally, an annual total of 23 Tg fluvial dissolved inorganic nitrogen (DIN) is transported to the continental shelf, of which $\sim 75\%$ escapes from the shelf to the open ocean (Jickells et al., 2017). Estuaries sit at the land-ocean interface, acting as natural reactors of multiple biogeochemical processes co-occurring in both water column and sediments (Crowe et al., 2012; Korth et al., 2013). For N cycling, this mainly involves assimilation, nitrification (ammonia oxidation: AO and nitrite oxidation: NO), denitrification, ammonification, anammox, nitrifier denitrification, coupled nitrification-denitrification, and even N_2 fixation (Altabet, 2006; Bentzon-Tilia et al., 2014; Casciotti, 2016b; Crowe et al., 2012; Granger et al., 2011; Wrage et al., 2001). Some of the above processes involve N_2O emission, a strong greenhouse gas, and thus link to climate issues. Despite the importance of in-estuary dynamics of N species (nitrate: NO_3^- , nitrite: NO_2^- , ammonium: NH_4^+ , dissolved organic nitrogen, and particulate nitrogen: PN), the full power of applying isotopic information to evaluate multiple co-occurring processes has only rarely been documented.

The traditional presentation of nutrient records in estuaries to examine the nonconservative behaviors (removal or addition) of N species relies on plotting N concentrations versus salinity to examine deviations from linearity (below or above the mixing line; Officer, 1979). This approach might miss biogeochemical processes when their impacts are balanced, for example, when NO_3^- production (nitrification) is balanced by

NO_3^- consumption (phytoplankton assimilation and/or microbial denitrification). Thus, concentrations alone present insufficient information to fully assess N transformations and may fail to reveal additional end-members and/or internal N transformation processes. Supplementary information provided by N isotope ($\delta^{15}\text{N}$) investigations in the Loire estuary have nicely demonstrated the limitations inherited in the classical two end-member mixing approach (Middelburg & Nieuwenhuize, 2001). The $\delta^{15}\text{N}$ provided specific aid in identifying N sources (Altabet, 2006; Wells et al., 2016; Yan et al., 2017), because $\delta^{15}\text{N}$ from different sources may have distinct isotopic compositions (Altabet, 2006; Casciotti, 2016a, 2016b). Moreover, N biological cycling often changes isotopic compositions in predictable and recognizable directions (Casciotti, 2016b; Sigman et al., 2009). For example, NO_3^- , NO_2^- , and NH_4^+ uptake by phytoplankton may result in significant enrichments in $\delta^{15}\text{N}$ of the remaining substrates due to isotope effects (Granger et al., 2010; K.-K. Liu et al., 2013; Waser et al., 1998). Importantly, the mixing of two end-members (two sources) will follow a straight line on the plot of $\delta^{15}\text{N}$ versus $1/[\text{N}]$ (Kendall et al., 2007), allowing identification of extra N sources or transformation pathways. The ability to resolve N sources and transformation pathways from observed chemical and isotopic gradients is also dependent on the water residence time (τ_w) in the estuary, that is, how rapidly microbial associated chemical processes can react in comparison to the time of travel under physical mixing.

In this study, we select the Jiulong River Estuary (JRE) as an archetype of macrotidal subtropical estuary to explore the dynamics of N processes along the salinity gradient and to examine to what degree various N transformations interact during downstream transport. The Jiulong River is characterized by approximately tenfold higher areal yield rate of NO_3^- ($>1,000 \text{ kg N km}^2 \text{ year}^{-1}$) than that of the Amazon River (Yan et al., 2012) as a result of intensive agriculture and pig/poultry farming (Chen & Hong, 2012; Yu et al., 2015). Although the spatial and temporal distributions of DIN (the sum of NO_3^- , NO_2^- , and NH_4^+) have been archived since the 1990s (Chen, 1985; Wu et al., 2017; Yan et al., 2012; Zhang et al., 1999), no previous isotopic study in the JRE has been conducted. According to the two end-member mixing model, the occurrence of significant NH_4^+ removal accompanying with NO_2^- addition has been observed in the upper JRE (Yan et al., 2012). The same phenomenon has been oft-observed in many worldwide estuaries, such as the Pearl River (Dai et al., 2008), the Danshuei River estuary (Wen et al., 2008), and the Elbe estuary (Sanders et al., 2017). Like some major estuaries, including the Loire estuary (Middelburg & Nieuwenhuize, 2001) and the Elbe estuary (Dähnke et al., 2008), however, NO_3^- plots conservatively versus salinity in the JRE (Yan et al., 2012). Thus, there appears to be no significant level of nitrification (unless it is balanced by assimilation and/or denitrification), despite the expectation that nitrification should occur rapidly in oxic water bodies (Altabet, 2006), especially in turbid estuary waters (Damashek et al., 2016).

To resolve the above issues, a field cruise was conducted across the environmental gradient in the JRE. To precisely decipher the mechanisms accounting for the spatial distributions of N species, we measured both concentrations (NH_4^+ , NO_3^- , NO_2^- , and PN) and isotopic compositions of multiple N species ($\delta^{15}\text{N}\text{-NO}_3^-$, $\delta^{18}\text{O}\text{-NO}_3^-$, $\delta^{15}\text{N}\text{-NO}_2^-$, and $\delta^{15}\text{N}\text{-PN}$). Incubation experiments concerning nitrification (including AO and NO) and N uptake were also conducted at selected stations. Accordingly, the oxidation rates and uptake rates were obtained and utilized to evaluate N behaviors in the JRE. This combination of incubation experiments with estuarine gradient observations is particularly powerful, because it allows comparison of the timescales required to generate chemical and isotopic signals to the timescales removed them. Specifically, in this study, the incubation results provide estimates of the timescales for NH_4^+ removal and NO_2^- accumulation ($\tau_{\text{ammonium-removal}}$ and $\tau_{\text{nitrite-accumulation}}$, respectively).

2. Materials and Methods

2.1. Study Area

The JRE is a macrotidal subtropical estuary located on the southwest coast of China in the Taiwan Strait, with a long-term mean water discharge of $1.4 \times 10^{10} \text{ m}^3/\text{year}$ (Huang, 2008). Due to the influence of subtropical monsoons, the river discharge is characterized by strong seasonal variations, with a maximum in May–June and minimum in November–January (Huang, 2008; Yan et al., 2012). The JRE is composed of North and South branches (Figure 1), and the latter is the main channel for water and sediment discharge (Luo et al., 1999). The JRE is a strong semidiurnal tidal estuary, with maximum tidal speed of $>2.0 \text{ m/s}$ in surface and $>1.5 \text{ m/s}$ at bottom (Cai et al., 1991). Both the high freshwater discharge in summer and the strong tides

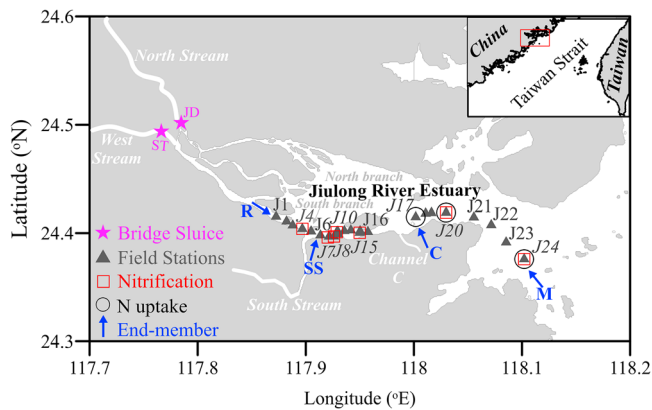


Figure 1. Map of Jiulong River Estuary and sampling stations. Black triangles represent stations with measurements of concentration and isotopic composition of N species, red squares are for incubation experiments of ammonia oxidation and nitrite oxidation (J4, J7, J8, J10, J15, J20, and J24), and black circles stand for incubation experiments of N uptake (J17, J20, and J24). Pink stars are bridge sluice. Blue arrows indicate the four end-members, including the riverine end-member (R), the SS end-member (the merging point of the South Stream), the C end-member (close to Channel C), and the marine end-member (M).

lead to rapid flushing of the estuary, and thus τ_w has been estimated to be <1 day based on ^{226}Ra data (Wang et al., 2015).

Resembling many other catchments, the Jiulong watershed is influenced by intensive anthropogenic activities (the catchment supports a total population of >3 million). Reportedly, the magnitudes of fertilizer application and livestock have increased by 6–10 times in recent decades (Chen & Hong, 2012). Meanwhile, more than 1,000 hydropower reservoirs have been constructed along the streams in the past 20 years (Meng, 2011), and accordingly, water retention and in-stream biological transformations (Chen et al., 2014) have been enhanced significantly. As a result, eutrophication and algal blooms had been observed more frequently in river and estuary waters (Li et al., 2011; Wu et al., 2017) threatening ecosystem stability. Diatoms have been reported to be the main phytoplankton species ($>80\%$) throughout the year in the JRE and exhibit clear seasonal variations with *Skeletonema costatum* dominant in summer and *Eucampia zodiacus* prevailing in spring (Wang et al., 2011).

The survey cruise was conducted using R/V Ocean II on 5 September 2016. A total of 24 locations (J1 to J24) were sampled to examine the spatial distributions and isotopic compositions of N species in the JRE (Figure 1). These sites were located along the main flow of the South Branch, extending from the riverine end-member (R; represented by

Station J1 with salinity of 0.7; Table 1) to the marine end-member (M; represented by Station J24 with salinity of 29.0; Table 1). Figure 1 also showed the location of two other important end-members (SS and C) along the estuary, which were identified from our observations as discussed in section 4.1. These four end-members divide the estuary into three sections: the upper estuary between R and SS, the middle estuary between SS and C, and the lower estuary between C and M. The locations of phytoplankton uptake and nitrification incubation experiments have also been shown in Figure 1.

2.2. Sampling

Water samples were taken from the water depth of ~ 0.5 m by using an organic glass hydrophore (1 L; Kedun Co., China) at each location (covering a salinity range of 0.7–29.0). In situ water temperature, salinity, and chlorophyll-*a* (Chl-*a*) were continuously measured (every 3 s, averaged to 1 min) by using a YSI6600D salinometer installed on an underway pumping system (Zhai et al., 2005). Salinities for samples were measured onboard using a portable multiparameter water quality analyzer (WTW, Multi 340i) based on conductivity measurements, with a precision of ± 0.1 (practical salinity units).

Approximately 200 ml water samples were filtered through polyether sulfone membrane filter (0.22 μm pore size; Millipore Express PES membrane, Merck) and the filtrates were stored frozen at -20°C for the analysis of DIN concentrations (NO_3^- , NO_2^- , and NH_4^+) and isotopic compositions ($\delta^{15}\text{N}-\text{NO}_3^-$, $\delta^{18}\text{O}-\text{NO}_3^-$, and $\delta^{15}\text{N}-\text{NO}_2^-$). An aliquot of 250 ml was collected and filtered for the measurement of total suspended solid (TSS) and PN (including $\delta^{15}\text{N}-\text{PN}$) using a 47-mm precombusted (450 $^\circ\text{C}$ for 4 hr) and preweighed glass fiber filter (0.7 μm pore size; GF/F, Whatman, GE Healthcare, USA) at a pressure of <100 mmHg. The GF/F filters were folded and wrapped in precombusted aluminum foil after MQ-water washing to remove salt and then were freeze-dried (CoolSafe Freeze Dryer, ScanVac) for 24 hr and stored in a vacuum desiccator for weighing (for TSS) and the analysis of PN and $\delta^{15}\text{N}-\text{PN}$.

2.3. Incubation Experiments

2.3.1. N Uptake/Absorption by Phytoplankton

The incubation experiments for uptake were conducted at three sites (J17, J20, and J24; Figure 1) in the middle-lower estuary with different salinity levels (19.8, 24.0, and 28.9, respectively). Duplicate water samples were collected in 10 L acid-washed transparent polycarbonate bottles

Table 1
The Compositions of Four End-Members

End-member	Salinity	NO_2^- ($\mu\text{mol/L}$)	NH_4^+ ($\mu\text{mol/L}$)	NO_3^- ($\mu\text{mol/L}$)
R	0.7	25.8	20.9	204.3
SS	6.5	33.9	9.8	165.0
C	20.3	13.2	13.8	76.8
M	29.0	6.3	6.5	22.9

Note. The R end-member was represented by the uppermost Station J1 due to its lowest salinity ($S = 0.7$). For M end-member, we selected the lowermost Station J24 as its highest salinity ($S = 29.0$).

(Nalgene, USA) from each site at near-surface depth (~0.5 m) using a diaphragm pump. One of them was subjected to continuous low-light (LL: $280 \pm 28 \mu\text{mol photons m}^{-2} \text{s}^{-1}$) while the others were incubated under continuous high light (HL: $714 \pm 26 \mu\text{mol photons m}^{-2} \text{s}^{-1}$), corresponding to the respective light levels of 20% and 50% of in situ highest surface photosynthetically active radiation (~1,450 $\mu\text{mol photons m}^{-2} \text{s}^{-1}$). The light was supplied by an Apollo-4 Full Spectrum source, and the light levels were measured by Delta OHM HD 2302.0 Light Meter. The incubations were cultured at room temperature (<30 °C) with constant illumination and monitored for 45–53 hr (until the NO_3^- concentration reached a plateau or was exhausted).

Initial subsamples (t_0) were collected prior to their different irradiance treatments for the analysis of N species (both concentration and isotopic composition). Subsequent subsamples were taken at discrete and increasing time intervals (4, 4, 8, 12, 12, and 12–19 hr). Water sample collections for the analyses of concentrations and isotopic compositions of N species during incubation experiments were similar to that of the field samples.

2.3.2. Ammonia Oxidation and Nitrite Oxidation

The incubation experiments of AO and NO were conducted at seven stations with different salinity and nutrient levels (Figure 1). The water samples were collected in a prewashed container (size: $30 \times 40 \times 70$ cm) from the surface layer (~0.5 m) using a diaphragm pump and then were separated into 250 ml high density polyethylene bottles for two parallel incubations. For AO rates, ^{15}N -label NH_4Cl tracer (different concentration gradient, containing 98 atom % ^{15}N , Sigma-Aldrich) was injected into each incubation bottle to avoid significantly changing ambient concentrations (<10%). Similarly, the supplement of ^{15}N -label NaNO_2 tracer (100 or 500 $\mu\text{mol/L}$, containing 98 atom % ^{15}N , Sigma-Aldrich) for NO rates was controlled to be ~10% of the observed NO_2^- . Initial subsamples (t_0) were filtered immediately after adding the tracers then the incubations were carried out in dark at simulated in situ temperature. Subsequent subsamples were taken at 6 (t_1) and 12 hr (t_2) for AO rates and at 6 and 28 hr for NO rates, respectively.

2.3.3. Rate Estimations From Incubation Results

Uptake rates were determined by the total N drawdown over elapsed time during the incubations. To ensure the accuracy of rate estimates, we considered only the time periods with linear decreases in N-concentrations. Thus, the first 21 hr was involved in the calculation of NH_4^+ uptake rate since it was rapidly consumed within this period. In contrast, the estimation of NO_3^- and NO_2^- uptake rates started from 15 hr since no obvious change was found in the concentration of NO_3^- and NO_2^- at the first 15 hr. All data from the HL and LL incubation experiments were combined to derive N uptake rates at each station, since they exhibited no statistically distinguishable differences.

Rates of AO and NO were determined by the net accumulation of ^{15}N in NO_2^- and NO_3^- , respectively (Ward, 2011). For this, we used a linear regression approach to obtain in situ reaction rates (three incubation time points, t_0 , t_1 , and t_2), as has been evaluated and applied in previous studies (Wan et al., 2018; Xu et al., 2018).

2.4. Analyses of Nitrogen Species Concentration

2.4.1. Dissolved Inorganic Nitrogen

Concentration of NO_3^- and NO_2^- were measured using an AA3 Auto-Analyzer (Bran+Luebbe Co., Germany), with a detection limit of 0.07 $\mu\text{mol/L}$ for NO_3^- and 0.02 $\mu\text{mol/L}$ for NO_2^- (Dai et al., 2008). Samples for NH_4^+ were analyzed based on indophenol blue spectrophotometric procedures (Pai et al., 2001), with a detection limit of 0.5 $\mu\text{mol/L}$.

2.4.2. Total Suspended Solid and Particulate Nitrogen

TSS concentrations were obtained by dividing the dry weight of particles on the GF/F filters by the volume of water filtered. After the weighing of TSS, these same GF/F filters were used to determine the concentrations of PN. PN was converted into NO_3^- using the “persulfate oxidation” method (Knapp et al., 2005), and its concentration was measured using the chemiluminescence method, with a detection limit of 0.05 $\mu\text{mol/L}$ (Knapp et al., 2005; Xu et al., 2017).

2.5. Isotopic Analyses

We determined $\delta^{15}\text{N}\text{-NO}_2^-$ by chemical conversion (sodium azide, Sigma, guaranteed reagent) of NO_2^- to nitrous oxide (N_2O), following McIlvin and Altabet (2005). In contrast, the dual isotopic compositions of

NO_3^- ($\delta^{15}\text{N}\text{-NO}_3^-$ and $\delta^{18}\text{O}\text{-NO}_3^-$) were measured by the denitrifier method (Casciott et al., 2002; Sigman et al., 2001), in which a denitrifying strain (*Pseudomonas aureofaciens*; ATCC# 13985) lacking the N_2O -reductase enzyme is used to quantitatively convert NO_3^- to N_2O . To avoid the influence of NO_2^- on the measurement of $\delta^{15}\text{N}\text{-NO}_3^-$ and $\delta^{18}\text{O}\text{-NO}_3^-$, preexisting NO_2^- in each sample was removed by adding sulfamic acid (Sigma, guaranteed reagent), following the detailed procedures in Granger and Sigman (2009). For $\delta^{15}\text{N}\text{-PN}$, PN were first oxidized to NO_3^- by using the above mentioned persulfate oxidation method, samples were then converted to N_2O by the denitrifier method. Subsequently, N_2O was extracted from sample vials, concentrated in liquid N_2 trap, and then separated with a gas chromatograph (GasBench II) for measurement in an Isotope Ratio Mass Spectrometer (Thermo Scientific DELTA V advantage).

Isotope ratios are reported using the delta (δ) notation in unit of per mil (‰) ($\delta = [\text{R}_{\text{sample}}/\text{R}_{\text{standard}} - 1] \times 1,000$, where $\text{R} = {}^{15}\text{N}/{}^{14}\text{N}$ or ${}^{18}\text{O}/{}^{16}\text{O}$). The ${}^{15}\text{N}/{}^{14}\text{N}$ standard is atmospheric N_2 , and the ${}^{18}\text{O}/{}^{16}\text{O}$ standard is Vienna-Standard Mean Ocean Water. The $\delta^{15}\text{N}\text{-NO}_3^-$ and $\delta^{18}\text{O}\text{-NO}_3^-$ were calibrated using laboratory working standards and international NO_3^- isotope standards, including IAEA-N3, USGS34, and USGS35 (the last one for $\delta^{18}\text{O}\text{-NO}_3^-$ only; Böhlke et al., 2003). The reproducibility for laboratory working standards was better than $\pm 0.2\%$ for both $\delta^{15}\text{N}\text{-NO}_3^-$ and $\delta^{18}\text{O}\text{-NO}_3^-$ (data from all batches conducted over 3 years). The analytical precisions of field samples for $\delta^{15}\text{N}\text{-NO}_3^-$ and $\delta^{18}\text{O}\text{-NO}_3^-$ in this study were better than $\pm 0.2\%$ and $\pm 0.5\%$, respectively, based on replicate measurements.

2.6. A Two End-Member Mixing Model

The mixing behavior of N species in estuaries is often assessed using a two end-member mixing model (Fry, 2002; Officer, 1979), and this approach has been widely applied in the tidal estuaries, such as the Scheldt estuary (Middelburg & Nieuwenhuize, 2001), the Elbe estuary (Dähnke et al., 2008), and the Pearl River estuary (Ye et al., 2015).

$$f_1 + f_2 = 1, \quad (1)$$

$$f_1 \times S_1 + f_2 \times S_2 = S_{\text{obs}}, \quad (2)$$

$$f_1 \times C_1 + f_2 \times C_2 = C_{\text{ex}}, \quad (3)$$

$$f_1 \times C_1 \times \delta_1 + f_2 \times C_2 \times \delta_2 = C_{\text{ex}} \times \delta_{\text{ex}}, \quad (4)$$

where C and δ denote, respectively, the concentration and isotopic composition of N species, the subscripts 1 and 2 indicate the two end-members. S represents salinity, and f denotes the water mixing ratio of two end-members in corresponding water sample. The subscripts obs and ex indicate, respectively, the observed values and expected values derived from mixing alone. Thus, any deviations between the observed and expected values in correspondence ($C_{\text{obs}} - C_{\text{ex}}$, denoted as “ C_{offset} ” hereafter) represent the signal of biological alteration (in situ consumption or production).

$$C_{\text{offset}} = C_{\text{obs}} - C_{\text{ex}}, \quad (5)$$

$$\delta_{\text{offset}} = \delta_{\text{obs}} - \delta_{\text{ex}}, \quad (6)$$

3. Results

3.1. Concentration Distribution of Nitrogen Species

Concentrations of NO_3^- exhibited a linear decrease along the salinity gradient (Figure 2a), nicely indicative of conservative mixing between eutrophic freshwater (R) and oligotrophic seawater (M). NO_3^- , as the main form of N in the JRE, was as high as $204 \mu\text{mol/L}$ at the estuary head and decreased to $23 \mu\text{mol/L}$ in the M end-member. Thus, from NO_3^- concentrations alone, no estuarine N transformations were evident.

Compared with NO_3^- , NO_2^- and NH_4^+ were at lower levels (<33.8 and $<20.7 \mu\text{mol/L}$, respectively) and showed totally different behaviors (Figure 2b). Interestingly, NO_2^- and NH_4^+ were nearly in mirror image with each other along the salinity gradient. In the upper estuary (between R and SS), the concentration of NO_2^- increased with salinity (salinity <4.0) and reached a plateau ($\sim 33.9 \mu\text{mol/L}$) when salinity was in the range of 4.0–8.2. The positive deviations from the R-M mixing line apparently suggested significant

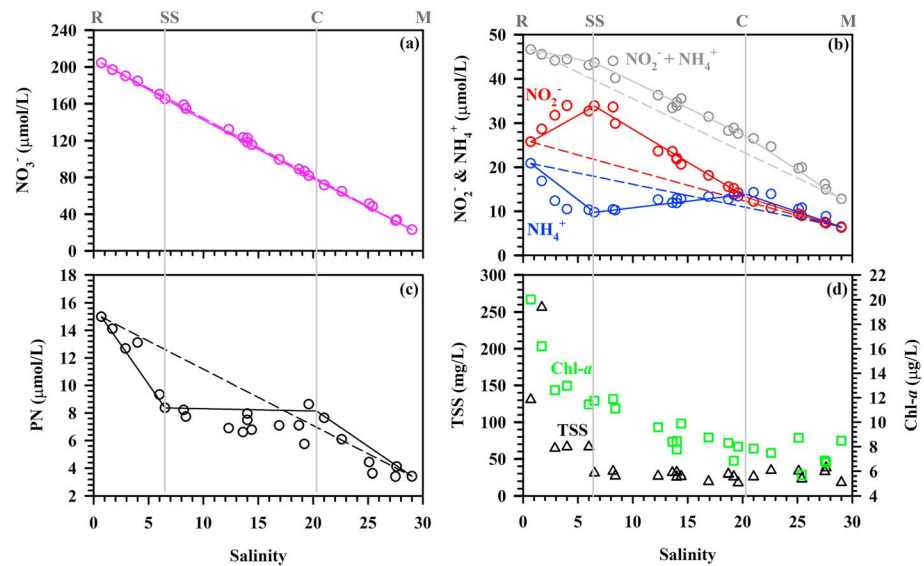


Figure 2. The variations of (a) NO_3^- , (b) NO_2^- and NH_4^+ , (c) PN, (d) Chl-*a* and TSS along the salinity gradient. The red and blue circles in (b) represent NO_2^- and NH_4^+ respectively, and the gray circles are for the sum of NO_2^- and NH_4^+ . The green squares and black triangles in (d) are Chl-*a* and TSS, respectively. The dash lines in (a), (b), and (c) represent the conservative mixing of freshwater (R) and seawater (M), while the solid lines stand for the mixing with two additional end-members (R and SS, SS and C, and C and M, respectively; see more details in section 4.1). PN = particulate nitrogen; SS = South Stream; TSS = total suspended solid.

NO_2^- accumulation. Correspondingly, NH_4^+ decreased to as low as $10.3 \mu\text{mol/L}$ around the salinity of 4.0 and remained near this level over the salinity range of 4.0–8.2. The negative deviations from the R-M mixing line indicated that NH_4^+ removal had occurred in the upper estuary. Notably, the positive NO_2^- offset was similar to the negative NH_4^+ offset in magnitude, implying that they might be connected by AO.

In the middle estuary (between SS and C), especially for salinity >8.2 , these trends reversed. NO_2^- declined while NH_4^+ increased until they were approximately equal near the C end-member. From this location onward NO_2^- declined approximately linearly to minimum in the M end-member. The behavior of NH_4^+ was similar, although in detail, NH_4^+ continued to increase slightly beyond C end-member reaching a maximum of $14.3 \mu\text{mol/L}$ at salinity of 21.0 and declined to $6.5 \mu\text{mol/L}$ in the M end-member. When looked into the fine scale of the R-M mixing line, the sum of NO_2^- and NH_4^+ reveals N addition along the entire salinity gradient (Figure 2b), suggesting processes other than AO might have occurred. The sharp variations in the scatter plot of NO_2^- (and NH_4^+) against salinity lead us to identify two new possible end-members at locations SS and C.

Broadly speaking, all three particulate matters (Chl-*a*, PN, and TSS) showed similar distributions, decreasing strongly downstream. But there were important differences. First, the magnitude of the decrease in Chl-*a* and PN was similar (approximately fivefold), which was much less than that of TSS (approximately tenfold). Second, the patterns of decrease were somewhat different. Chl-*a* showed an exponential-like decrease with salinity that continued across the whole estuary (Figure 2d). The highest Chl-*a* ($20 \mu\text{g/L}$) occurred in the upper estuary under conditions of the highest turbidity rather than the lower estuary, suggesting the importance of allochthonous Chl-*a* input from upper stream (e.g., from JD and/or ST bridge sluices/reservoirs, Figure 1). In contrast, while the PN concentration decreased similarly to that of Chl-*a* in the upper estuary, it then remained relatively constant in the middle estuary before decreasing more strongly in the lower estuary (Figure 2c). Interestingly, the PN pattern was very similar to that of NH_4^+ (compare Figures 2b and 2c) suggesting that certain processes associated with particles (e.g., absorption/desorption or release during sediment resuspension) link them. For TSS, essentially all of the decrease occurred in the upper estuary. In detail, the highest TSS (256 mg/L) was observed when salinity was 1.7 rather than 0.7 (Figure 2d). This approximately twofold higher TSS was likely induced by the resuspension of coarse mineral grains, since PN for this sample was not elevated. TSS then decreased rapidly from 131 to 31 mg/L at salinity of 6.5 or so, and then stayed at a constant low level of 20–35 mg/L toward the sea.

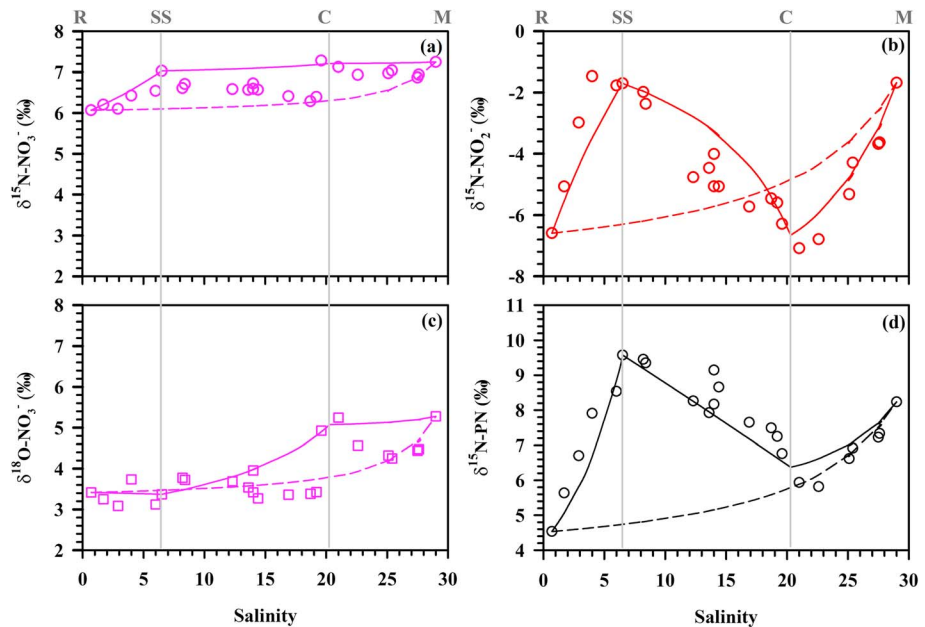


Figure 3. The variations of (a) $\delta^{15}\text{N-NO}_3^-$, (b) $\delta^{15}\text{N-NO}_2^-$, (c) $\delta^{18}\text{O-NO}_3^-$, (d) $\delta^{15}\text{N-PN}$ along the salinity gradient. The dash lines in (a), (b), and (c) represent the conservative mixing of R and M end-members, while the solid lines are three specific mixing lines (R-SS, SS-C, and C-M) for four end-members. SS = South Stream.

3.2. Isotopic Compositions of Nitrogen Species

The isotopic compositions of NO_3^- , NO_2^- , and PN were shown in Figure 3. The $\delta^{15}\text{N}$ variations in NO_3^- were smallest ($\sim 1\text{‰}$), ranging from 6.1‰ in the R end-member to 7.2‰ at the M end-member (Figure 3a). Notably, throughout the estuary, $\delta^{15}\text{N-NO}_3^-$ fell slightly above the conservative R-M mixing line. There were local maxima near both SS (7.0‰) and C (7.2‰) end-members. Overall, the variations of $\delta^{18}\text{O-NO}_3^-$ were somewhat larger ($\sim 2\text{‰}$), ranging from 3.1‰ to 5.3‰ throughout the estuary (Figure 3c). As with $\delta^{15}\text{N-NO}_3^-$, there was a local maximum in $\delta^{18}\text{O-NO}_3^-$ near C end-member, but in contrast, there was no local maximum near SS end-member. Importantly, these fine scale variations are close to the detection limitations for NO_3^- dual isotopes. Thus, caution is required in their interpretation.

$\delta^{15}\text{N-NO}_2^-$ showed a much greater variation of 5.6‰, ranging from -7.1‰ to -1.5‰ (Figure 3b). It exhibited an N-shaped pattern along the salinity gradient and dramatically deviated from the R-M mixing line. Again, the SS and C locations stood out, reemphasizing their likely role as additional sources, but in different ways than for NO_3^- . There was a strong maximum (-1.7‰) at SS end-member (similar to the M end-member) but a strong minimum (-7.1‰) at C end-member (slightly lower than the R end-member).

$\delta^{15}\text{N-PN}$ exhibited a very similar range (5.1‰) and an almost identical N-shaped pattern to that of $\delta^{15}\text{N-NO}_2^-$ (Figure 3d), with the overall minimum at the R end-member (4.5‰) and a strong minimum near C end-member (5.8‰). The overall maximum occurred at SS end-member (9.6‰), exceeding the M end-member (8.2‰). The similarity of the $\delta^{15}\text{N-PN}$ and $\delta^{15}\text{N-NO}_2^-$ variations strongly suggested that they were linked by their sources and/or the processes that modify them in the estuary.

3.3. Incubation Experiments

Although we set two light intensities for incubation, there were no obvious differences between the HL and LL treatments for either concentrations or isotopic compositions (Figure 4). This was because the irradiance of LL treatment was already saturated for phytoplankton growth. The saturating light threshold of 140–150 $\mu\text{mol photons m}^{-2} \text{s}^{-1}$ was generally applied previously for both the laboratory monocultures (Granger et al., 2004; Needoba & Harrison, 2004) and the natural marine plankton consortium (Rohde et al., 2015). Thus, the HL and LL treatments are considered as duplicate samples hereafter.

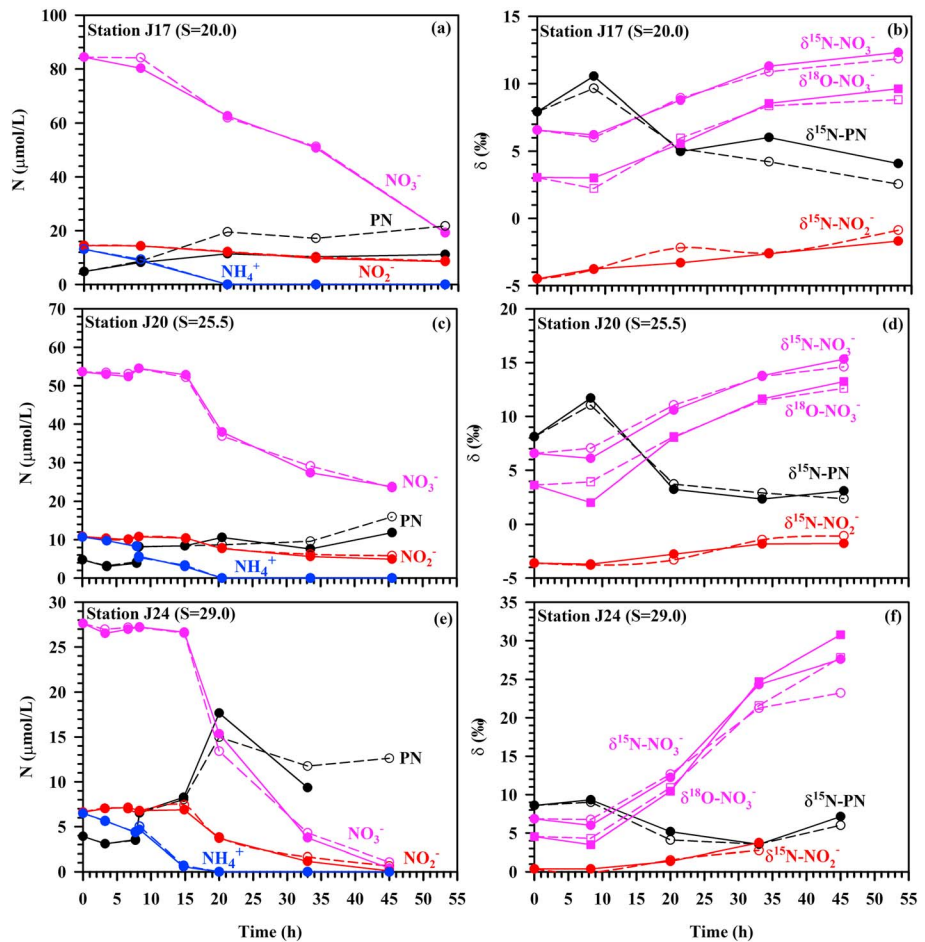


Figure 4. The time courses of nitrogen concentrations and isotopic compositions during incubation experiments at Stations J17 (a and b), J20 (c and d), and J24 (e and f) under high and low light. $\delta^{15}\text{N-NO}_2^-$ values at the last time point were not shown in (f) since NO_2^- concentration was too low for isotope measurement. PN = particulate nitrogen.

At Station J17 (Figure 4a), NH_4^+ declined quickly at the beginning of incubation and was exhausted in 21 hr, with a total drawdown of $\sim 13 \mu\text{mol/L}$. However, no detectable change of NO_2^- was found in the first 8 hr, and after time point, NO_2^- began to decrease and fell to $8.5\text{--}8.7 \mu\text{mol/L}$ at the end of incubation. Correspondingly, $\delta^{15}\text{N-NO}_2^-$ increased from -4.5‰ to around -1.3‰ . Similar to NO_2^- , NO_3^- did not show obvious change in the first 8 hr; however, it declined quickly afterward with a total drawdown of $\sim 65.0 \mu\text{mol/L}$ in the end. Correspondingly, $\delta^{15}\text{N-NO}_3^-$ and $\delta^{18}\text{O-NO}_3^-$ increased significantly after 8 hr (Figure 4b), with maximum value of 12.0‰ for $\delta^{15}\text{N-NO}_3^-$ and 9.2‰ for $\delta^{18}\text{O-NO}_3^-$, respectively. PN rapidly increased in the first 21 hr, then it varied in a range of $10.3\text{--}21.7 \mu\text{mol/L}$ until the end of incubation. Obviously, such increment of PN ($6.6\text{--}16.9 \mu\text{mol/L}$) was in response to the uptake of NH_4^+ , NO_2^- , and NO_3^- . Noteworthy, the temporal variations of $\delta^{15}\text{N-PN}$ was more complex. At the early stage of incubations, $\delta^{15}\text{N-PN}$ rose rapidly (from 7.9‰ to 10.6‰) and exceeded $\delta^{15}\text{N-NO}_3^-$ ($6.0\text{‰}\text{--}6.6\text{‰}$) suggesting that PN originated as phytoplankton growing on NH_4^+ with elevated $\delta^{15}\text{N-PN}$ of about $8\text{‰}\text{--}11\text{‰}$ and thus suggesting this is a likely minimum estimate for $\delta^{15}\text{N-NH}_4^+$ without considering the isotope effect. After NH_4^+ depletion, $\delta^{15}\text{N-PN}$ dropped strongly, consistent with the switch to growth on NO_3^- and NO_2^- . At this stage, $\delta^{15}\text{N-PN}$ lowered than $\delta^{15}\text{N-NO}_3^-$ but exceeded $\delta^{15}\text{N-NO}_2^-$ due to the combination of the isotope effects during uptake and lower $\delta^{15}\text{N}$ in NO_3^- and NO_2^- relative to NH_4^+ .

Similar trends of N species and their isotopic compositions were found at Station J20 (Figures 4c and 4d). A total drawdown of NH_4^+ , NO_2^- , and NO_3^- were 10.7 , 5.5 , and $35.8 \mu\text{mol/L}$ in average, respectively. Meanwhile, variations of $\delta^{15}\text{N}$ (both pattern and magnitude) were similar to that of Station J17. For PN, it

increased by 7.0–11.2 $\mu\text{mol/L}$ over the course of incubations, in the same level with that of incubation at Station J17.

At Station J24 (Figures 4e and 4f), the trends of NH_4^+ , NO_2^- , and NO_3^- were similar to the other two sites. However, both NO_3^- and NO_2^- were exhausted at the end of incubations, with a total consumption of ~ 26.8 and ~ 6.2 $\mu\text{mol/L}$, respectively. Both $\delta^{15}\text{N-NO}_3^-$ and $\delta^{18}\text{O-NO}_3^-$ increased sharply after 8 hr, consistent with Stations J17 and J20. However, the values of $\delta^{15}\text{N-NO}_3^-$ and $\delta^{18}\text{O-NO}_3^-$ at the end of incubations were significantly higher than that of other two stations, with values of 23.2‰–27.6‰ and 27.8‰–30.7‰, respectively. Similarly, obvious increasing trends can be found in $\delta^{15}\text{N-NO}_2^-$, with an increment of around 2.4‰–3.3‰ over the course of incubations. Interestingly, PN sharply rose up to 15.0–17.7 $\mu\text{mol/L}$ during 18–21 hr; after 21 hr, it began to decrease to 9.3–11.7 $\mu\text{mol/L}$. Note that, $\delta^{15}\text{N-PN}$ slightly increased (0.4‰–0.7‰) in the first 8 hr, and it began to decrease (~ 3.5 ‰) afterward quickly until 33 hr. At the last time point, it increased back to the level of 6.0‰–7.1‰.

Generally, three incubation experiments yielded similar results. NH_4^+ was drawn down steadily from the start and exhausted after 20 hr or sooner. Little consumption of NO_3^- and NO_2^- occurred until after NH_4^+ was exhausted and then proceeded in parallel. The $\delta^{15}\text{N}$ of dissolved N species all increased as expected for residual substrates undergoing the isotope effects during assimilation.

4. Discussion

Our observations raise several important scientific questions: (1) Why does $\delta^{15}\text{N-NO}_2^-$ rather than $\delta^{15}\text{N-NO}_3^-$ was used to identify N sources in the JRE? (2) In the upper estuary (R to SS), NH_4^+ was significantly consumed while NO_2^- was accumulated. Does this reflect significant and rapid estuarine oxidation of NH_4^+ to NO_2^- ? (3) Does the conservative behavior exhibit by NO_3^- in the whole estuary result from the strong physical mixing and/or the NH_4^+ suppression effect on NO_3^- uptake? In the sections that follow, we address these questions.

4.1. Nitrite Isotopes Reveal Two Extra End-Members

The uptake rate of NH_4^+ in light was up to 11.8 ± 0.7 $\mu\text{mol L}^{-1} \text{day}^{-1}$ at Station J17 (Table 2), similar to Station J20 (12.5 ± 1.4 $\mu\text{mol L}^{-1} \text{day}^{-1}$) but slightly higher than that of Station J24 (9.1 ± 1.0 $\mu\text{mol L}^{-1} \text{day}^{-1}$). Note that NH_4^+ was exhausted in the first 15 hr for all incubation experiments, whereas both NO_2^- and NO_3^- were not assimilated during this period. This overall suggests that phytoplankton has strong preference for NH_4^+ over NO_2^- and NO_3^- , consistent with previous studies (McCarthy et al., 1977; Middelburg & Nieuwenhuize, 2000; Xu et al., 2017), of which phytoplankton need extra energy for NO_3^- and NO_2^- reduction to NH_4^+ and thus prefer NH_4^+ (Lomas & Lipschultz, 2006). In this “classical physiological perspective,” NO_3^- and NO_2^- uptake are inhibited by NH_4^+ above the threshold of 1–4 $\mu\text{mol/L}$ (Conway et al., 1976; Glibert et al., 2015).

After the exhaustion of NH_4^+ , phytoplankton turned to assimilate NO_3^- and NO_2^- simultaneously, with the uptake rates of 19.2–30.0 $\mu\text{mol L}^{-1} \text{day}^{-1}$ and 2.9–5.0 $\mu\text{mol L}^{-1} \text{day}^{-1}$, respectively. The uptake rates of NO_2^- were about 10%–25% of NO_3^- . Although the uptake rate of NO_3^- was the highest among three DIN sources, we cannot detect any removal signal of NO_3^- within the JRE (Figure 2a). This may be attributed to the suppression of NH_4^+ on NO_3^- assimilation, since NH_4^+ was in a high level of >6.5 $\mu\text{mol/L}$. Similar inhibition effect was found for NO_2^- uptake in incubations. According to such inhibition, both $\delta^{15}\text{N-NO}_3^-$ (including $\delta^{18}\text{O-NO}_3^-$) and $\delta^{15}\text{N-NO}_2^-$ can be useful tools to trace N sources in the JRE due to low influences of biological isotope fraction. Unfortunately, the variation ranges of $\delta^{15}\text{N-NO}_3^-$ and $\delta^{18}\text{O-NO}_3^-$ in the JRE were narrow (<1 ‰–2‰) and thus made it difficult to effectively trace NO_3^- sources. Of course, a plausible explanation of this is that the NO_3^- pool in the JRE was too large to be altered by biological processes since τ_w in the JRE is as short as <1 day in summer (Wang et al., 2015). The low impact of biological transformations in rapidly flushed estuary has been noted before in the Tweed estuary (Ahad et al., 2006).

On the other hand, $\delta^{15}\text{N-NO}_2^-$ was variable, ranging from -7.1 ‰ to -1.5 ‰. NO_2^- is a metastable intermediate, and thus, multiple processes cause NO_2^- to have a shorter turnover time relative to NO_3^- (Middelburg & Nieuwenhuize, 2000; Wells et al., 2016), accordingly distinct $\delta^{15}\text{N-NO}_2^-$ end-member values may indicate an ongoing supply originating from different sources. The relatively low concentration of NO_2^-

Table 2
The Uptake Rates of NH_4^+ , NO_2^- , and NO_3^- by Phytoplankton in Light (Unit: $\mu\text{mol L}^{-1}\text{day}^{-1}$)

Station	Salinity	NH_4^+	NO_2^-	NO_3^-
J17	20.0	11.8 ± 0.7	2.9 ± 0.2	30.0 ± 1.7^b
J20	25.5	12.5 ± 1.4	3.6 ± 0.7^b	20.6 ± 3.4
J24	29.0	9.1 ± 1.0^a	5.0 ± 0.7^b	19.2 ± 3.1^c

Note. The N uptake rates were derived from the slope of the regression line in Figures 4a, 4c, and 4e, respectively. *p* values of the above estimation of rates were lower than 0.0001, except for those with subscripts a (*p* = 0.0041), b (*p* = 0.0010), and c (*p* = 0.0008).

facilitated the evident impact of extra end-members even though τ_w was short. Similarly, $\delta^{15}\text{N-NO}_2^-$ provided better constraints on identifying N sources and processes in the open ocean (Buchwald & Casciotti, 2013; Casciotti, 2016a) and the groundwater system (Wells et al., 2016).

To further explore N dynamics in the JRE, we drew a scatter plot of $\delta^{15}\text{N-NO}_2^-$ against $1/[\text{NO}_2^-]$ (Figure 5), in which a straight line reveals control by two end-member mixing (Kendall et al., 2007). In the JRE, it exhibited a distinctive N-shaped pattern, which can be thought of as three specific mixing lines (R-SS, SS-C, and C-M). In other words, except for the R and M end-members, there were two

other end-members (SS and C), one characterized by high $\delta^{15}\text{N-NO}_2^-$ whereas the other featured by low $\delta^{15}\text{N-NO}_2^-$. According to the sampling locations (Figure 1), we suggested that the former end-member was sourced from the South Stream (SS) merging into the main channel of JRE. Thus, Station J6 located in proximity to the entry of SS was selected as the SS end-member, which was characterized with the highest NO_2^- , $\delta^{15}\text{N-NO}_2^-$, and $\delta^{15}\text{N-PN}$ values. A possible explanation for the high $\delta^{15}\text{N-PN}$ is that PN coming down from the SS had been influenced by phytoplankton assimilation of NH_4^+ (with high $\delta^{15}\text{N-NH}_4^+$). It was consistent with its lower NH_4^+ concentration and TSS levels (lower turbidity and thus higher light to drive production). While high $\delta^{15}\text{N-NO}_2^-$ is difficult to explain, likely reduction processes were involved. Since the SS end-member did not provide significant freshwater input, we also speculated that τ_w is longer in the south stream due to its lower water discharge. The second end-member was located nearby the outlet of Channel C, which extends inland toward a high-density local industry area, including feed mills, metallurgical factories, and other businesses. Moreover, a large amount of bivalve aquaculture is carried out nearby (just inshore to the south of Stations J18–J20). Therefore, we averaged values of Stations J17 and J18 for the C end-member. Although the C and R end-members exhibited similar $\delta^{15}\text{N-NO}_2^-$ and $\delta^{15}\text{N-PN}$, the former had lower particle loads since it was mainly influenced by local industries rather than turbid riverine inputs. Moreover, salinity for C end-member was significantly higher than R end-member, suggesting that τ_w was much longer in adjacent brackish shallow waters nearby Channel C. The compositions of the above four end-members were summarized in Table 1. Additionally, the theoretical mixing lines of four end-members were shown by solid lines in Figures 2 and 3.

4.2. Shifted N Transformation Processes Downstream

To distinguish biological processes from physical mixing, a two end-member mixing model was applied to obtain C_{offset} and δ_{offset} (see more details in section 2.6), to reflect the biogeochemical influences/alterations.

The C_{offset} and δ_{offset} values combined with rates of oxidation and uptake allowed us to further unravel the dynamics of N species in the JRE. A similar offset method has been successfully applied to assess N dynamics in large estuaries and plumes, such as the Pearl River plume (Han et al., 2012) and the Yangtze River plume (Yan et al., 2017).

4.2.1. Oxidation Dominated Ammonium Consumption in the Upper Estuary

After recognizing the mixing of R and SS end-members in the upper estuary, we derived $[\text{NO}_2^-]_{\text{offset}}$ and $[\text{NH}_4^+]_{\text{offset}}$ for this section (Table S1 in the supporting information). Results showed that the absolute magnitude of $[\text{NO}_2^-]_{\text{offset}}$ (+1.5 to +3.6 $\mu\text{mol/L}$) was slightly lower than that of $[\text{NH}_4^+]_{\text{offset}}$ (−2.1 to −4.3 $\mu\text{mol/L}$). This is consistent with some onward oxidation of NO_2^- to NO_3^- as expected from the rates of AO (R_{AO}), NO (R_{NO}), and NH_4^+ uptake in dark (R_{AUD}) calculated from the incubation experiments (Table 3). In the upper estuary (Station J4), R_{AO} was as high as 20.4 $\mu\text{mol L}^{-1}\text{day}^{-1}$, which was twentyfold higher than R_{NO} (1.0 $\mu\text{mol L}^{-1}\text{day}^{-1}$). Previous study has found that nitrite oxidation bacteria are more sensitive to salinity relative to ammonia oxidation bacteria (Pronk et al., 2014). The differential sensitivity to salinity may be a plausible

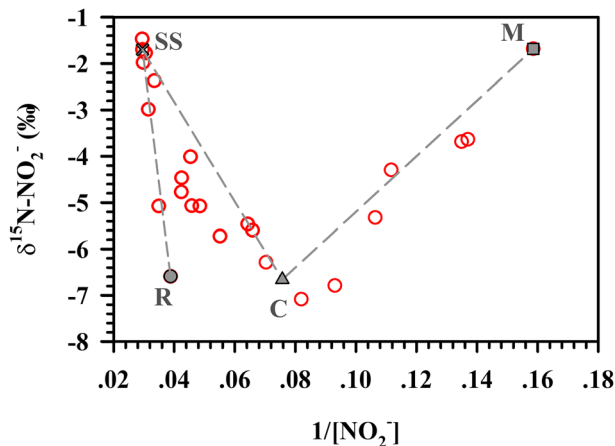


Figure 5. Scatter plot of $\delta^{15}\text{N-NO}_2^-$ versus $1/[\text{NO}_2^-]$. Gray dot, cross, triangle, and square are four end-members (R, SS, C, and M, respectively). SS = South Stream.

Table 3
Rates of Ammonia Oxidation, Nitrite Oxidation, Ammonium Uptake in the Dark (Unit: $\mu\text{mol L}^{-1} \text{day}^{-1}$)

Station	Ammonia oxidation (R_{AO})	Nitrite oxidation (R_{NO})	Ammonium uptake in dark (R_{AUD})
J4	20.4 ± 0.6	1.0 ± 0.0	3.3 ± 0.0
J7	2.5 ± 0.0	0.3 ± 0.0	/
J8	0.4 ± 0.0	0.0 ± 0.0	2.1 ± 0.0
J10	0.4 ± 0.0	0.1 ± 0.0	/
J15	0.1 ± 0.0	0.0 ± 0.0	/
J20	0.2 ± 0.0	0.0 ± 0.0	/
J24	0.5 ± 0.0	0.0 ± 0.0	0.9 ± 0.0

reason for NO_2^- accumulation in the upper estuary, consistent with the study in the wastewater treatment (Zhao et al., 2014). Generally, AO can decrease $\delta^{15}\text{N-NO}_2^-$ due to the isotope effect of -14‰ to -38‰ (Casciotti et al., 2003; Santoro & Casciotti, 2011). However, in the upper estuary where AO was the highest, a positive isotope-offset of NO_2^- ($+0.3\text{‰}$ to $+2.0\text{‰}$) was found, suggesting that AO slightly increased $\delta^{15}\text{N-NO}_2^-$. This only can be explained by higher $\delta^{15}\text{N-NH}_4^+$ relative to $\delta^{15}\text{N-NO}_2^-$. That is supported by the incubations which showed that $\delta^{15}\text{N-PN}$ started to decrease when phytoplankton switch to growth on NO_3^- and NO_2^- as NH_4^+ was exhausted (see section 3.3 and Figure 4). R_{AO} and R_{NO} peaked in the upper estuary where TSS was high. High concentrations of suspended particle may both provide substrate NH_4^+ to nitrifiers (Hsiao et al., 2014; Wang et al., 2010; Zheng et al., 2017) and protect nitrifiers from light damage (Liltved & Cripps, 1999). The weak salinity tolerance of nitrifying bacteria communities (Bernhard et al., 2007; Morrissey et al., 2014) is an additional possible reason for low nitrification in high salinity sites. In addition to removal by oxidation, it was possible that some NH_4^+ could be assimilated by heterotrophic microbes (i.e., nitrifiers), which was consistent with the uptake rate of NH_4^+ in dark (R_{AUD}) of $3.3 \mu\text{mol L}^{-1} \text{day}^{-1}$ (Table 3). Although NH_4^+ assimilation by phytoplankton could explain NH_4^+ loss, it would be limited by high TSS in the upper estuary (Figure 2d).

To estimate the timescale for NH_4^+ removal ($\tau_{\text{ammonium_removal}}$), we divided $[\text{NH}_4^+]_{\text{offset}}$ by the summed rates of NH_4^+ removal ($R_{\text{AO}}+R_{\text{AUD}}$). Similarly, for $\tau_{\text{nitrite_accumulation}}$, $[\text{NO}_2^-]_{\text{offset}}$ was divided by the rates of NO_2^- production and removal ($R_{\text{AO}}-R_{\text{NO}}$). These two turnover times showed similar ranges of 2–5 hr and were thus significantly shorter than previously reported water residence time of <19 hr (Wang et al., 2015), consistent with previous findings in the European tidal estuaries (Middelburg & Nieuwenhuize, 2000, 2001). Thus, our estimated rates were coherent with the nonconservative behaviors observed in our NH_4^+ and NO_2^- versus salinity plots (Figure 2b).

Relative to $[\text{NH}_4^+]_{\text{offset}}$ and $[\text{NO}_2^-]_{\text{offset}}$, the values of $[\text{NO}_3^-]_{\text{offset}}$ were much smaller (-0.6 to $+2.7 \mu\text{mol/L}$; Table S1) accounting for only 0.3%–1.5% of the observed NO_3^- pool. This suggested that turnover time for NO_3^- pool was much longer than the water residence time and, thus, consistent with the conservative behavior of NO_3^- with salinity (Figure 2a). This result was also supported by the negligible isotope-offsets (0.1%–0.4%, close to our analytical uncertainty). Alternatively, NO_3^- production can be compensated by NO_3^- consumption in term of concentration and isotopic composition. Although nitrification can contribute to NO_3^- production, it was minor given the observed low NO rates (Table 3). As aforementioned, NO_3^- assimilation by phytoplankton had been inhibited by high turbidity and NH_4^+ levels (NH_4^+ repression of NO_3^-). Meanwhile, denitrification in the water column should be negligible due to high levels of dissolved oxygen (Wang et al., 2015). Although denitrification may occur in sediments (Lehmann et al., 2004; Prokopenko et al., 2011), in our case, the influence of sedimentary denitrification on the surface water NO_3^- appears to have been limited since no NO_3^- removal was observed in the upper estuary. One may argue that incomplete denitrification may happen due to strong tidal mixing, yet the positive shifts in dual isotopes of NO_3^- were very small in our case. As for the denitrification occurring on suspended particles (T. Liu et al., 2013; Yao et al., 2016), it may play a vital role when TSS was high, such as $\text{TSS} > 2.5 \text{ g/L}$ (T. Liu, et al., 2013). But TSS in this study was $< 0.1 \text{ g/L}$ and, thus, its influences should be minor, consistent with previous study in Poyang lake (Yao et al., 2016).

The influences of submarine water discharge on the water column NH_4^+ and NO_2^- were not directly evaluated in our case. In accord with the rapid water flushing time, however, its impact is likely to be limited by the relatively small spatial-averaged source of reported groundwater input (Hong et al., 2017; Wang et al., 2015). Due to low oxygen in groundwater, coupled nitrification-denitrification prevails with values of $\delta^{15}\text{N-NO}_3^-$ (-3‰ to $+60\text{‰}$) and $\delta^{18}\text{O-NO}_3^-$ (0‰ to $+50\text{‰}$; Wells et al., 2016) that can be significantly higher than riverine/marine sources. Because only minimal increments were observed in $\delta^{15}\text{N-NO}_3^-$ and $\delta^{18}\text{O-NO}_3^-$ in the JRE (and limited to the SS and C end-members), it appears that there were negligible influences from submarine water discharge at least during this period of the year.

4.2.2. The Causes for Nitrate Conservation in the Middle and Lower Estuary

Following the same procedure in section 4.2.1, the $[\text{NH}_4^+]_{\text{offset}}$, $[\text{NO}_2^-]_{\text{offset}}$, and $[\text{NO}_3^-]_{\text{offset}}$ were derived in the middle (SS-C) and lower estuary (C-M). Results were supportive of the fact that physical mixing dominated the distributions of N species in the middle and lower estuary since the offsets of N species only occupied a small fraction of the observed values (<8%, within the error of determination). This was consistent with lower rates of AO and NO in the middle and lower estuary (Table 3), possibly resulting from inhibition by the higher salinity (Gonzalez-Silva et al., 2016; Mannina et al., 2016) and/or sunlight (Horak et al., 2017; Liltved & Cripps, 1999; Xu et al., 2019) due to lack of shading by TSS.

Under the lower TSS conditions of the middle and lower estuary, N assimilation by phytoplankton should become more significant since the growth of phytoplankton is no longer limited by light. In our incubation experiments, we found high uptake rates of N species in the middle and lower reach (Table 2). Using our NH_4^+ uptake rates of $9.1\text{--}12.5 \mu\text{mol L}^{-1} \text{day}^{-1}$ in the light (Table 2) and $0.9 \mu\text{mol L}^{-1} \text{day}^{-1}$ in the dark (Table 3), and assuming in a 12-hr light: 12-hr dark cycle, the daily total removal of NH_4^+ was estimated to be as high as $5\text{--}6 \mu\text{mol/L}$ in the middle and lower estuary. This suggested that the observed NH_4^+ ($6.5\text{--}14.3 \mu\text{mol/L}$) should be removed completely within 1–3 days. However, NH_4^+ remained close to conservative in the middle and lower estuary (Figure 2b). This suggests that the τ_w was considerably <1 day in this area, which was consistent with results ($\tau_w = 0.78$ day) calculated using radium isotopes in summer (Wang et al., 2015).

Finally, we note that in addition to physical mixing, the high level of NH_4^+ throughout the JRE also can contribute to the conservative behavior of NO_3^- through repressing NO_3^- uptake by phytoplankton. Although NH_4^+ inhibition effect has been documented in both cultures (Conway et al., 1976; Syrett & Morris, 1963) and field observations (Dugdale et al., 2007; McCarthy et al., 1977), its roles on the conservative behaviors of NO_3^- in estuaries has rarely been reported. Our isotope labelling and natural abundance observations emphasized that NH_4^+ repression of NO_3^- uptake should be considered when discussing NO_3^- dynamics in field studies. Otherwise, we may overestimate the influence of physical mixing on N dynamics in estuaries with high NH_4^+ .

Worldwide, anthropogenic activities are not only increasing total N inputs (Seitzinger & Harrison, 2008; Sharples et al., 2017) but also shifting the dominant form of N (Glibert et al., 2006, 2014; Lee et al., 2014) delivered to estuaries and coastal areas. In fact, substantially elevated concentrations of NH_4^+ are common in many estuaries, such as the Maryland/Virginia Coastal Lagoon (Glibert et al., 2014) and the Danshuei estuary (Lee et al., 2014). This is attributable to the development of animal agriculture and marine aquaculture which produce high NH_4^+ by direct excretion and/or decomposition of undigested feed (Bouwman et al., 2013; Zhang et al., 2015).

Under these conditions, NH_4^+ inhibition effects could become more significant in estuaries and coastal areas. This can alter phytoplankton community structure and thus further affect biogeochemical cycles and ecological processes (Shilova et al., 2017). Understanding the processes which remove NH_4^+ and their dependence on particle loads, light levels, salinity, and estuarine dynamics is therefore of increasing importance. The combination of natural abundance isotopic surveys with rate studies from tracer incubations is a powerful approach to assess this issue.

5. Conclusions

1. The N-shaped patterns in the downstream distributions of the isotopic compositions of NO_2^- and PN, and in the scatter plot of $\delta^{15}\text{N}\text{-NO}_2^-$ versus $1/[\text{NO}_2^-]$, suggested that the involvement of four (R, SS, C, and M end-members) rather than two end-members (R and M end-members) in the JRE.
2. Significant shifts in the relative importance of different N transformation processes were found across the environmental gradients. In the upper estuary (where turbidity was high), rate of AO was as high as $20.4 \mu\text{mol L}^{-1} \text{day}^{-1}$, which was twentyfold higher than NO. This huge difference between rates of AO and NO led to significant NH_4^+ removal and NO_2^- accumulation in the upper estuary. In contrast, in the middle and lower estuary, the influences of biological processes (both oxidation and uptake) were less evident and were largely overwhelmed by strong physical mixing.

3. According to the incubation experiments for N uptake, phytoplankton expressed strong preference of NH_4^+ over NO_3^- and NO_2^- , suggesting the repression of NO_3^- uptake by NH_4^+ . This inhibition effect occurred at NH_4^+ levels as low as $0.6 \mu\text{mol/L}$, contributing to the conservative behavior of NO_3^- and the small variability in the dual isotopes of NO_3^- along the JRE.
4. Based on the rapid NH_4^+ consumption in the incubations, a residence time of less than 1 day was required to maintain the conservative mixing behavior of NH_4^+ in the middle-lower estuary.

Acknowledgments

We thank Qiaoyun Lin, Qian Zhu, and Yanhua Wu for their help in water sampling. This work was supported by the National Natural Science Foundation of China (41806092, 41721005, 41561164019, 41503069, and 91851209) and the Shantou University Scientific Research Foundation for Talents (NTF18013). All data in this study were listed in the supporting information (Tables S1–S2). The authors declare that they have no known competing financial interests or personal relationships that could have appeared to influence the work reported in this paper.

References

- Ahad, J. M. E., Ganeshram, R. S., Spencer, R. G. M., Uher, G., Upstill-Goddard, R. C., & Cowie, G. L. (2006). Evaluating the sources and fate of anthropogenic dissolved inorganic nitrogen (DIN) in two contrasting North Sea estuaries. *Science of the Total Environment*, *372*(1), 317–333. <https://doi.org/10.1016/j.scitotenv.2006.09.018>
- Altabet, M. A. (2006). Isotopic tracers of the marine nitrogen cycle: Present and past. In J. Volkman (Ed.), *Marine organic matter: Chemical and biological markers* (pp. 251–293). Berlin, Heidelberg: Springer-Verlag. https://doi.org/10.1007/698_2_008
- Bentzon-Tilia, M., Traving, S. J., Mantikci, M., Knudsen-Leerbeck, H., Hansen, J. L. S., Markager, S., & Riemann, L. (2014). Significant N_2 fixation by heterotrophs, photoheterotrophs and heterocystous cyanobacteria in two temperate estuaries. *The ISME Journal*, *9*(2), 273–285. <https://doi.org/10.1038/ismej.2014.119>
- Bernhard, A. E., Tucker, J., Giblin, A. E., & Stahl, D. A. (2007). Functionally distinct communities of ammonia-oxidizing bacteria along an estuarine salinity gradient. *Environmental Microbiology*, *9*(6), 1439–1447. <https://doi.org/10.1111/j.1462-2920.2007.01260.x>
- Böhlke, J. K., Mroczkowski, S. J., & Coplen, T. B. (2003). Oxygen isotopes in nitrate: New reference materials for ^{18}O : ^{16}O measurements and observations on nitrate-water equilibration. *Rapid Communications in Mass Spectrometry*, *17*(16), 1835–1846. <https://doi.org/10.1002/rcm.1123>
- Bouwman, L., Beusen, A., Glibert, P. M., Overbeek, C., Pawlowski, M., Herrera, J., et al. (2013). Mariculture: Significant and expanding cause of coastal nutrient enrichment. *Environmental Research Letters*, *8*(4), 925–932. <https://doi.org/10.1088/1748-9326/8/4/044026>
- Buchwald, C., & Casciotti, K. L. (2013). Isotopic ratios of nitrite as tracers of the sources and age of oceanic nitrite. *Nature Geoscience*, *6*(4), 308–313. <https://doi.org/10.1038/ngeo1745>
- Cai, A. Z., Cai, Y. E., Zhun, X. N., Cai, X., Chen, J. M., & Zhang, Y. M. (1991). Diffusion and modern sedimentation of seaward-transporting discharges in the estuary of Jiulongjiang River, Fujian Province (in Chinese). *Marine Geology & Quaternary Geology (Beijing)*, *11*, 57–67.
- Casciotti, K. L., Sigman, D. M., Hastings, M. G., Böhlke, J. K., & Hilker, A. (2002). Measurement of the oxygen isotopic composition of nitrate in seawater and freshwater using the denitrifier method. *Analytical Chemistry*, *74*(19), 4905–4912. <https://doi.org/10.1021/ac020113w>
- Casciotti, K. L. (2016a). Nitrite isotopes as tracers of marine N cycle processes. *Philosophical Transactions of the Royal Society A: Mathematical, Physical and Engineering Sciences*, *374*(2081). <https://doi.org/10.1098/rsta.2015.0295>
- Casciotti, K. L. (2016b). Nitrogen and oxygen isotopic studies of the marine nitrogen cycle. *Annual Reviews of Marine Science*, *8*(1), 379–407. <https://doi.org/10.1146/annurev-marine-010213-135052>
- Casciotti, K. L., Sigman, D. M., & Ward, B. B. (2003). Linking diversity and stable isotope fractionation in ammonia-oxidizing bacteria. *Geomicrobiology Journal*, *20*(4), 335–353. <https://doi.org/10.1080/01490450303895>
- Chen, N., & Hong, H. (2012). Integrated management of nutrients from the watershed to coast in the subtropical region. *Current Opinion in Environmental Sustainability*, *4*(2), 233–242. <https://doi.org/10.1016/j.cosust.2012.03.007>
- Chen, N., Wu, Y., Wu, J., Yan, X., & Hong, H. (2014). Natural and human influences on dissolved silica export from watershed to coast in Southeast China. *Journal of Geophysical Research: Biogeosciences*, *119*, 95–109. <https://doi.org/10.1002/2013jg002429>
- Chen, S. T. (1985). Chemical characteristics of nutrient elements in the Jiulong Estuary and the calculation of its flux (in Chinese). *Journal of Tropical Oceanography*, *4*, 16–24.
- Conway, H. L., Harrison, P. J., & Davis, C. O. (1976). Marine diatoms grown in chemostats under silicate or ammonium limitation. II. Transient response of *Skeletonema costatum* to a single addition of the limiting nutrient. *Marine Biology*, *35*(2), 187–199. <https://doi.org/10.1007/bf00390940>
- Crowe, S. A., Canfield, D. E., Mucci, A., Sundby, B., & Maranger, R. (2012). Anammox, denitrification and fixed-nitrogen removal in sediments from the Lower St. Lawrence Estuary. *Biogeosciences*, *9*(11), 4309–4321. <https://doi.org/10.5194/bg-9-4309-2012>
- Dähnke, K., Bahlmann, E., & Emeis, K. (2008). A nitrate sink in estuaries? An assessment by means of stable nitrate isotopes in the Elbe estuary. *Limnology and Oceanography*, *53*(4), 1504–1511. <https://doi.org/10.4319/lo.2008.53.4.1504>
- Dai, M., Wang, L., Guo, X., Zhai, W., He, B., & Kao, S. J. (2008). Nitrification and inorganic nitrogen distribution in a large perturbed river/estuarine system: The Pearl River Estuary, China. *Biogeosciences*, *5*(5), 1227–1244. <https://doi.org/10.5194/bg-5-1227-2008>
- Damashek, J., Casciotti, K. L., & Francis, C. A. (2016). Variable nitrification rates across environmental gradients in turbid, nutrient-rich estuary waters of San Francisco Bay. *Estuaries and Coasts*, *39*(4), 1050–1071. <https://doi.org/10.1007/s12237-016-0071-7>
- Dugdale, R. C., Wilkerson, F. P., Hogue, V. E., & Marchi, A. (2007). The role of ammonium and nitrate in spring bloom development in San Francisco Bay. *Estuarine, Coastal and Shelf Science*, *73*(1–2), 17–29. <https://doi.org/10.1016/j.ecss.2006.12.008>
- Fry, B. (2002). Conservative mixing of stable isotopes across estuarine salinity gradients: A conceptual framework for monitoring watershed influences on downstream fisheries production. *Estuaries*, *25*(2), 264–271. <https://doi.org/10.1007/BF02691313>
- Glibert, P. M., Harrison, J., Heil, C., & Seitzinger, S. (2006). Escalating worldwide use of urea—A global change contributing to coastal eutrophication. *Biogeochemistry*, *77*(3), 441–463. <https://doi.org/10.1007/s10533-005-3070-5>
- Glibert, P. M., Hinkle, D. C., Sturgis, B., & Jesien, R. V. (2014). Eutrophication of a Maryland/Virginia coastal lagoon: A tipping point, ecosystem changes, and potential causes. *Estuaries and Coasts*, *37*(S1), 128–146. <https://doi.org/10.1007/s12237-013-9630-3>
- Glibert, P. M., Wilkerson, F. P., Dugdale, R. C., Raven, J. A., Dupont, C. L., Leavitt, P. R., et al. (2015). Pluses and minuses of ammonium and nitrate uptake and assimilation by phytoplankton and implications for productivity and community composition, with emphasis on nitrogen-enriched conditions. *Limnology and Oceanography*, *61*(1), 165–197. <https://doi.org/10.1002/lno.10203>
- Gonzalez-Silva, B. M., Jonassen, K. R., Bakke, I., Ostgaard, K., & Vadstein, O. (2016). Nitrification at different salinities: Biofilm community composition and physiological plasticity. *Water Research*, *95*, 48–58. <https://doi.org/10.1016/j.watres.2016.02.050>

- Granger, J., Prokopenko, M. G., Sigman, D. M., Mordy, C. W., Morse, Z. M., Morales, L. V., et al. (2011). Coupled nitrification-denitrification in sediment of the eastern Bering Sea shelf leads to ^{15}N enrichment of fixed N in shelf waters. *Journal of Geophysical Research*, *116*, C11006. <https://doi.org/10.1029/2010JC006751>
- Granger, J., & Sigman, D. M. (2009). Removal of nitrite with sulfamic acid for nitrate N and O isotope analysis with the denitrifier method. *Rapid Communications in Mass Spectrometry*, *23*(23), 3753–3762. <https://doi.org/10.1002/rcm.4307>
- Granger, J., Sigman, D. M., Needoba, J. A., & Harrison, P. J. (2004). Coupled nitrogen and oxygen isotope fractionation of nitrate during assimilation by cultures of marine phytoplankton. *Limnology and Oceanography*, *49*(5), 1763–1773. <https://doi.org/10.4319/lo.2004.49.5.1763>
- Granger, J., Sigman, D. M., Rohde, M. M., Maldonado, M. T., & Tortell, P. D. (2010). N and O isotope effects during nitrate assimilation by unicellular prokaryotic and eukaryotic plankton cultures. *Geochimica et Cosmochimica Acta*, *74*(3), 1030–1040. <https://doi.org/10.1016/j.gca.2009.10.044>
- Han, A., Dai, M., Kao, S.-J., Gan, J., Li, Q., Wang, L., et al. (2012). Nutrient dynamics and biological consumption in a large continental shelf system under the influence of both a river plume and coastal upwelling. *Limnology and Oceanography*, *57*(2), 486–502. <https://doi.org/10.4319/lo.2012.57.2.0486>
- Hong, Q., Cai, P., Shi, X., Li, Q., & Wang, G. (2017). Solute transport into the Jiulong River estuary via pore water exchange and submarine groundwater discharge: New insights from $^{224}\text{Ra}/^{228}\text{Th}$ disequilibrium. *Geochimica et Cosmochimica Acta*, *198*, 338–359. <https://doi.org/10.1016/j.gca.2016.11.002>
- Horak, R. E. A., Qin, W., Bertagnolli, A. D., Nelson, A., Heal, K. R., Han, H., et al. (2017). Relative impacts of light, temperature, and reactive oxygen on thaumarchaeal ammonia oxidation in the North Pacific Ocean. *Limnology and Oceanography*, *63*(2), 741–757. <https://doi.org/10.1002/lno.10665>
- Hsiao, S. S.-Y., Hsu, T.-C., Liu, J.-w., Xie, X., Zhang, Y., Lin, J., et al. (2014). Nitrification and its oxygen consumption along the turbid Chang Jiang River plume. *Biogeosciences*, *11*(7), 2083–2098. <https://doi.org/10.5194/bg-11-2083-2014>
- Huang, X. Q. (2008). Hydrological characteristics in the Jiulong watershed (in Chinese). *Hydraulic Science and Technology*, *1*, 16–20.
- Jickells, T. D., Buitenhuis, E., Altieri, K., Baker, A. R., Capone, D., Duce, R. A., et al. (2017). A reevaluation of the magnitude and impacts of anthropogenic atmospheric nitrogen inputs on the ocean. *Global Biogeochemical Cycles*, *31*, 289–305. <https://doi.org/10.1002/2016GB005586>
- Kendall, C., Elliott, E. M., & Wankel, S. D. (2007). Tracing anthropogenic inputs of nitrogen to ecosystems. In M. Robert & L. Kate (Eds.), *Stable Isotopes in Ecology and Environmental Science* (pp. 375–449).
- Knapp, A. N., Sigman, D. M., & Lipschultz, F. (2005). N isotopic composition of dissolved organic nitrogen and nitrate at the Bermuda Atlantic Time-series Study site. *Global Biogeochemical Cycles*, *19*, GB1018. <https://doi.org/10.1029/2004GB002320>
- Korth, F., Fry, B., Liskow, L., & Voss, M. (2013). Nitrogen turnover during the spring outflows of the nitrate-rich Curonian and Szczecin lagoons using dual nitrate isotopes. *Marine Chemistry*, *154*, 1–11. <https://doi.org/10.1016/j.marchem.2013.04.012>
- Lee, T. Y., Shih, Y. T., Huang, J. C., Kao, S. J., Shiah, F. K., & Liu, K. K. (2014). Speciation and dynamics of dissolved inorganic nitrogen export in the Danshui River, Taiwan. *Biogeosciences*, *11*(19), 5307–5321. <https://doi.org/10.5194/bg-11-5307-2014>
- Lehmann, M. F., Sigman, D. M., & Berelson, W. M. (2004). Coupling the $^{15}\text{N}/^{14}\text{N}$ and $^{18}\text{O}/^{16}\text{O}$ of nitrate as a constraint on benthic nitrogen cycling. *Marine Chemistry*, *88*(1–2), 1–20. <https://doi.org/10.1016/j.marchem.2004.02.001>
- Li, Y., Cao, W., Su, C., & Hong, H. (2011). Nutrient sources and composition of recent algal blooms and eutrophication in the northern Jiulong River, Southeast China. *Marine Pollution Bulletin*, *63*(5–12), 249–254. <https://doi.org/10.1016/j.marpolbul.2011.02.021>
- Liltved, H., & Cripps, S. J. (1999). Removal of particle-associated bacteria by prefiltration and ultraviolet irradiation. *Aquaculture Research*, *30*(6), 445–450. <https://doi.org/10.1046/j.1365-2109.1999.00349.x>
- Liu, K.-K., Kao, S.-J., Chiang, K.-P., Gong, G.-C., Chang, J., Cheng, J.-S., & Lan, C. Y. (2013). Concentration dependent nitrogen isotope fractionation during ammonium uptake by phytoplankton under an algal bloom condition in the Danshuei estuary, northern Taiwan. *Marine Chemistry*, *157*, 242–252. <https://doi.org/10.1016/j.marchem.2013.10.005>
- Liu, T., Xia, X., Liu, S., Mou, X., & Qiu, Y. (2013). Acceleration of denitrification in turbid rivers due to denitrification occurring on suspended sediment in oxic waters. *Environmental Science & Technology*, *47*(9), 4053–4061. <https://doi.org/10.1021/es304504m>
- Lomas, M. W., & Lipschultz, F. (2006). Forming the primary nitrite maximum: Nitrifiers or phytoplankton? *Limnology and Oceanography*, *51*(5), 2453–2467. <https://doi.org/10.4319/lo.2006.51.5.2453>
- Luo, J., Gong, J., & Zhang, X. (1999). Multitemporal analyses of remote sensing on distribution, transportation and sedimentation of suspended sediment in the Jiulongjiang Mouth and Xiamen Estuary (in Chinese). *Journal of Nanjing Hydraulic Research Institute*, *4*, 368–376.
- Mannina, G., Capodici, M., Cosenza, A., Di Trapani, D., & Viviani, G. (2016). Sequential batch membrane bio-reactor for wastewater treatment: The effect of increased salinity. *Bioresour Technol*, *209*, 205–212. <https://doi.org/10.1016/j.biortech.2016.02.122>
- McCarthy, J. J., Taylor, W. R., & Taft, J. L. (1977). Nitrogenous nutrition of the plankton in the Chesapeake Bay. 1. Nutrient availability and phytoplankton preferences. *Limnology and Oceanography*, *22*(6), 996–1011. <https://doi.org/10.4319/lo.1977.22.6.0996>
- McIlvin, M. R., & Altabet, M. A. (2005). Chemical conversion of nitrate and nitrite to nitrous oxide for nitrogen and oxygen isotopic analysis in freshwater and seawater. *Analytical Chemistry*, *77*(17), 5589–5595. <https://doi.org/10.1021/ac050528s>
- Meng, D. (2011). Thousands of minitype hydropower stations do harm to the Jiulong River, Fujian (in Chinese). *Water Carriage Pearl River*, *44*, 44–47.
- Middelburg, J., & Nieuwenhuize, J. (2001). Nitrogen isotope tracing of dissolved inorganic nitrogen behaviour in tidal estuaries. *Estuarine, Coastal and Shelf Science*, *53*(3), 385–391. <https://doi.org/10.1006/eccs.2001.0805>
- Middelburg, J. J., & Nieuwenhuize, J. (2000). Uptake of dissolved inorganic nitrogen in turbid, tidal estuaries. *Marine Ecology Progress*, *192*(1), 79–88.
- Moore, C. M., Mills, M. M., Arrigo, K. R., Berman-Frank, I., Bopp, L., Boyd, P. W., et al. (2013). Processes and patterns of oceanic nutrient limitation. *Nature Geoscience*, *1*(4), 210–210. <https://doi.org/10.1038/ngeo176>
- Morrissey, E. M., Gillespie, J. L., Morina, J. C., & Franklin, R. B. (2014). Salinity affects microbial activity and soil organic matter content in tidal wetlands. *Global Change Biology*, *20*(4), 1351–1362. <https://doi.org/10.1111/gcb.12431>
- Needoba, J. A., & Harrison, P. J. (2004). Influence of low light and a light:dark cycle on NO_3^- uptake, intracellular NO_3^- , and nitrogen isotope fractionation by marine phytoplankton. *Journal of Phycology*, *40*(3), 505–516. <https://doi.org/10.1111/j.1529-8817.2004.03171.x>
- Officer, C. B. (1979). Discussion of the behaviour of nonconservative dissolved constituents in estuaries. *Estuarine and Coastal Marine Science*, *9*(1), 91–94. [https://doi.org/10.1016/0302-3524\(79\)90009-4](https://doi.org/10.1016/0302-3524(79)90009-4)
- Pai, S. C., Tsau, Y.-J., & Yang, T.-I. (2001). pH and buffering capacity problems involved in the determination of ammonia in saline water using the indophenol blue spectrophotometric method. *Analytica Chimica Acta*, *434*(2), 209–216. [https://doi.org/10.1016/S0003-2670\(01\)00851-0](https://doi.org/10.1016/S0003-2670(01)00851-0)

- Prokopenko, M. G., Sigman, D. M., Berelson, W. M., Hammond, D. E., Barnett, B., Chong, L., & Townsend-Small, A. (2011). Denitrification in anoxic sediments supported by biological nitrate transport. *Geochimica et Cosmochimica Acta*, 75(22), 7180–7199. <https://doi.org/10.1016/j.gca.2011.09.023>
- Pronk, M., Bassin, J. P., de Kreuk, M. K., Kleerebezem, R., & van Loosdrecht, M. C. (2014). Evaluating the main and side effects of high salinity on aerobic granular sludge. *Applied Microbiology and Biotechnology*, 98(3), 1339–1348. <https://doi.org/10.1007/s00253-013-4912-z>
- Rohde, M. M., Granger, J., Sigman, D. M., & Lehmann, M. F. (2015). Coupled nitrate N and O stable isotope fractionation by a natural marine plankton consortium. *Frontiers in Marine Science*, 2(1-13). <https://doi.org/10.3389/fmars.2015.00028>
- Sanders, T., Schöl, A., & Dähnke, K. (2017). Hot spots of nitrification in the Elbe estuary and their impact on nitrate regeneration. *Estuaries and Coasts*, 41(1), 128–138. <https://doi.org/10.1007/s12237-017-0264-8>
- Santoro, A. E., & Casciotti, K. L. (2011). Enrichment and characterization of ammonia-oxidizing archaea from the open ocean: Phylogeny, physiology and stable isotope fractionation. *ISME J*, 5(11), 1796–1808. <https://doi.org/10.1038/ismej.2011.58>
- Seitzinger, S. P., & Harrison, J. A. (2008). Chapter 9—Land-based nitrogen sources and their delivery to coastal systems. In *Nitrogen in Marine Environment* (pp. 469–510). Elsevier Science & Technology.
- Sharples, J., Middelburg, J. J., Fennel, K., & Jickells, T. D. (2017). What proportion of riverine nutrients reaches the open ocean? *Global Biogeochemical Cycles*, 31, 39–58. <https://doi.org/10.1002/2016GB005483>
- Shilova, I. N., Mills, M. M., Robidart, J. C., Turk-Kubo, K. A., Björkman, K. M., Kolber, Z., et al. (2017). Differential effects of nitrate, ammonium, and urea as N sources for microbial communities in the North Pacific Ocean. *Limnology and Oceanography*, 62(6), 2550–2574. <https://doi.org/10.1002/lno.10590>
- Sigman, D. M., Casciotti, K. L., Andreani, M., Barford, C., Galanter, M., & Bohlke, J. K. (2001). A bacterial method for the nitrogen isotopic analysis of nitrate in seawater and freshwater. *Analytical Chemistry*, 73(17), 4145–4153. <https://doi.org/10.1021/ac010088e>
- Sigman, D. M., Karsh, K. L., & Casciotti, K. L. (2009). *Ocean process tracers: Nitrogen isotopes in the ocean*, *Encyclopedia of Ocean Sciences* (pp. 4138–4153).
- Syrett, P. J., & Morris, I. (1963). The inhibition of nitrate assimilation by ammonium in chlorella. *Biochimica et Biophysica Acta*, 67, 566–575. [https://doi.org/10.1016/0926-6569\(63\)90277-3](https://doi.org/10.1016/0926-6569(63)90277-3)
- Wan, X. S., Sheng, H. X., Dai, M., Zhang, Y., Shi, D., Trull, T. W., et al. (2018). Ambient nitrate switches the ammonium consumption pathway in the euphotic ocean. *Nature Communication*, 9(1), 915. <https://doi.org/10.1038/s41467-018-03363-0>
- Wang, G., Wang, Z., Zhai, W., Moore, W. S., Li, Q., Yan, X., et al. (2015). Net subterranean estuarine export fluxes of dissolved inorganic C, N, P, Si, and total alkalinity into the Jiulong River estuary, China. *Geochimica et Cosmochimica Acta*, 149, 103–114. <https://doi.org/10.1016/j.gca.2014.11.001>
- Wang, H., Shen, Z., Guo, X., Niu, J., & Kang, B. (2010). Ammonia adsorption and nitrification in sediments derived from the Three Gorges Reservoir, China. *Environmental Earth Sciences*, 60(8), 1653–1660. <https://doi.org/10.1007/s12665-009-0299-7>
- Wang, Y., Lin, M., Chen, X. Q., & Lin, G. M. (2011). Spatial and temporal variation of phytoplankton and impacting factors in Jiulongjiang Estuary of Xiamen, China (in Chinese). *Acta Ecologica Sinica*, 31(12), 3399–3414.
- Ward, B. B. (2011). Measurement and distribution of nitrification rates in the oceans. *Methods in Enzymology*, 486, 307–323. <https://doi.org/10.1016/B978-0-12-381294-0.00013-4>
- Waser, N., Harrison, P., Nielsen, B., Calvert, S., & Turpin, D. (1998). Nitrogen isotope fractionation during the uptake and assimilation of nitrate, nitrite, ammonium, and urea by a marine diatom. *Limnology and Oceanography*, 43(2), 215–224. <https://doi.org/10.4319/lo.1998.43.2.0215>
- Wells, N. S., Hakoun, V., Brouyere, S., & Knoller, K. (2016). Multi-species measurements of nitrogen isotopic composition reveal the spatial constraints and biological drivers of ammonium attenuation across a highly contaminated groundwater system. *Water Research*, 98, 363–375. <https://doi.org/10.1016/j.watres.2016.04.025>
- Wen, L.-S., Jiann, K.-T., & Liu, K.-K. (2008). Seasonal variation and flux of dissolved nutrients in the Danshuei Estuary, Taiwan: A hypoxic subtropical mountain river. *Estuarine, Coastal and Shelf Science*, 78(4), 694–704. <https://doi.org/10.1016/j.ecss.2008.02.011>
- Wrage, N., Velthof, G. L., van Beusichem, M. L., & Oenema, O. (2001). Role of nitrifier denitrification in the production of nitrous oxide. *Soil Biology and Biochemistry*, 33(12-13), 1723–1732. [https://doi.org/10.1016/S0038-0717\(01\)00096-7](https://doi.org/10.1016/S0038-0717(01)00096-7)
- Wu, G., Cao, W., Huang, Z., Kao, C.-M., Chang, C.-T., Chiang, P.-C., & Wang, F. (2017). Decadal changes in nutrient fluxes and environmental effects in the Jiulong River Estuary. *Marine Pollution Bulletin*, 124(2), 871–877. <https://doi.org/10.1016/j.marpolbul.2017.01.071>
- Xu, M. N., Li, X., Shi, D., Zhang, Y., Dai, M., Huang, T., et al. (2019). Coupled effect of substrate and light on assimilation and oxidation of regenerated nitrogen in the euphotic ocean. *Limnology and Oceanography*, 64(3), 1270–1283. <https://doi.org/10.1002/lno.11114>
- Xu, M. N., Wu, Y., Zheng, L. W., Zheng, Z., Zhao, H., Laws, E. A., & Kao, S. J. (2017). Quantification of multiple simultaneously occurring nitrogen flows in the euphotic ocean. *Biogeosciences*, 14(4), 1021–1038. <https://doi.org/10.5194/bg-14-1021-2017>
- Xu, M. N., Zhang, W., Zhu, Y., Liu, L., Zheng, Z., Wan, X. S., et al. (2018). Enhanced ammonia oxidation caused by lateral Kuroshio intrusion in the boundary zone of the northern South China Sea. *Geophysical Research Letters*, 45, 6585–6593. <https://doi.org/10.1029/2018GL077896>
- Yan, X., Xu, M. N., Wan, X. S., Yang, J.-Y. T., Trull, T. W., Dai, M., & Kao, S. J. (2017). Dual isotope measurements reveal zoning of nitrate processing in the summer Changjiang (Yangtze) River Plume. *Geophysical Research Letters*, 44, 12,289–12,297. <https://doi.org/10.1002/2017GL075951>
- Yan, X., Zhai, W., Hong, H., Li, Y., Guo, W., & Huang, X. (2012). Distribution, fluxes and decadal changes of nutrients in the Jiulong River Estuary, Southwest Taiwan Strait. *Chinese Science Bulletin*, 57(18), 2307–2318. <https://doi.org/10.1007/s11434-012-5084-4>
- Yao, X., Zhang, L., Zhang, Y., Xu, H., & Jiang, X. (2016). Denitrification occurring on suspended sediment in a large, shallow, subtropical lake (Poyang Lake, China). *Environmental Pollution*, 219, 501–511. <https://doi.org/10.1016/j.envpol.2016.05.073>
- Ye, F., Ni, Z., Xie, L., Wei, G., & Jia, G. (2015). Isotopic evidence for the turnover of biological reactive nitrogen in the Pearl River Estuary, south China. *Journal of Geophysical Research: Biogeosciences*, 120, 661–672. <https://doi.org/10.1002/2014jg002842>
- Yu, D., Yan, W., Chen, N., Peng, B., Hong, H., & Zhuo, G. (2015). Modeling increased riverine nitrogen export: Source tracking and integrated watershed-coast management. *Marine Pollution Bulletin*, 101(2), 642–652. <https://doi.org/10.1016/j.marpolbul.2015.10.035>
- Zhai, W., Dai, M., Cai, W.-J., Wang, Y., & Wang, Z. (2005). High partial pressure of CO₂ and its maintaining mechanism in a subtropical estuary: The Pearl River estuary, China. *Marine Chemistry*, 93(1), 21–32. <https://doi.org/10.1016/j.marchem.2004.07.003>
- Zhang, Y., Bleeker, A., & Liu, J. (2015). Nutrient discharge from China's aquaculture industry and associated environmental impacts. *Environmental Research Letters*, 10(4), S109. <https://doi.org/10.1088/1748-9326/10/4/045002>

- Zhang, Y. H., Wang, W. Q., & Huang, Z. Q. (1999). Salinity fronts and chemical behaviour of nutrient in Jiulongjiang Estuary (in Chinese). *Marine Environmentalence*, 4, 1–7.
- Zhao, W., Wang, Y., Lin, X., Zhou, D., Pan, M., & Yang, J. (2014). Identification of the salinity effect on N₂O production pathway during nitrification: Using stepwise inhibition and ¹⁵N isotope labeling methods. *Chemical Engineering Journal*, 253, 418–426. <https://doi.org/10.1016/j.cej.2014.05.052>
- Zheng, Z. Z., Wan, X., Xu, M. N., Hsiao, S. S. Y., Zhang, Y., Zheng, L. W., et al. (2017). Effects of temperature and particles on nitrification in a eutrophic coastal bay in southern China. *Journal of Geophysical Research: Biogeosciences*, 122, 2325–2337. <https://doi.org/10.1002/2017JG003871>